

Cell shape and intercellular adhesion regulate mitotic spindle orientation

Jingchen Li, Longcan Cheng, and Hongyuan Jiang*

CAS Key Laboratory of Mechanical Behavior and Design of Materials, Hefei National Laboratory for Physical Science at the Microscale, Department of Modern Mechanics, CAS Center for Excellence in Complex System Mechanics, University of Science and Technology of China, Hefei, Anhui 230026, China

ABSTRACT Cell division orientation plays an essential role in tissue morphogenesis and cell fate decision. Recent studies showed that either cell shape or adhesion geometry can regulate the orientation of mitotic spindles and thereby the cell division orientation. However, how they together regulate the spindle orientation remains largely unclear. In this work, we use a general computational model to investigate the competitive mechanism of determining the spindle orientation between cell shape and intercellular adhesion in epithelial cells. We find the spindle orientation is dominated by the intercellular adhesion when the cell shape anisotropy is small, but dominated by the cell shape when the shape anisotropy is large. A strong adhesion and moderate adhesive size can ensure the planar division of epithelial cells with large apico-basal elongation. We also find the spindle orientation could be perpendicular to the adhesive region when only one side of the cell is adhered to an E-cadherin-coated matrix. But after the cell is compressed, the spindle orientation is governed by the cell shape and the spindle will be parallel to the adhesive region when the cell shape anisotropy is large. Finally, we demonstrate the competition between cell shape and tricellular junctions can also effectively regulate the spindle orientation.

Monitoring Editor
Alex Mogilner
New York University

Received: Apr 23, 2019
Revised: Jun 26, 2019
Accepted: Jul 29, 2019

INTRODUCTION

The orientation of the cell-division axis determines the positions of daughter cells in a tissue and thereby is crucial to the tissue morphogenesis and cell fate decisions (Théry and Bornens, 2006; di Pietro *et al.*, 2016). Misoriented cell division can result in various developmental disorders (Gillies and Cabernard, 2011; Williams *et al.*, 2011; Lancaster and Knoblich, 2012) and may also be responsible for the tumor progression (Causinus and Gonzalez, 2005; Pease and Tirnauer, 2011; Nakajima *et al.*, 2013). Cell division orientation is coupled to the mitotic spindle orientation. More than 100 years ago, the cell shape had been thought of as a determinant of spindle

orientation, which is known as the "long axis rule" (Hertwig, 1884). Recent studies also confirmed the correlation between the cell shape and the spindle orientation (O'Connell and Wang, 2000; Strauss *et al.*, 2006; Minc *et al.*, 2011; Xiong *et al.*, 2014; Li and Jiang, 2018). However, in many frequently used systems, the adhesion geometry (Théry *et al.*, 2005, 2007; Matsumura *et al.*, 2016), cell polarity (Siller and Doe, 2009; Williams and Fuchs, 2013), or extracellular mechanical force (Fink *et al.*, 2011; Hart *et al.*, 2017; Scarpa *et al.*, 2018; Finegan *et al.*, 2019) sometimes could override the cell shape to determine the spindle orientation.

In general, the long axis of the interphase cell is consistent with the principal direction of the extracellular force or anisotropic adhesion, because these factors can elongate the cell during the interphase (Théry *et al.*, 2005; Fink *et al.*, 2011; Wyatt *et al.*, 2015; Bosveld *et al.*, 2016). Therefore, the spindle orientation is usually along the long axis of the cell as well as the principal direction of extracellular force or adhesion. It is difficult to distinguish their individual influences on the spindle orientation.

However, this is not always the case. Recent experiments have found some cues about the competition between the cell shape and adhesion. For example, the division of epithelia is usually planar, that is, parallel to the monolayer plane, to maintain the single-layered tissue architecture (Ragkousi and Gibson, 2014)

This article was published online ahead of print in MBoC in Press (<http://www.molbiolcell.org/cgi/doi/10.1091/mbc.E19-04-0227>) on August 14, 2019.

Author contributions: H.J. initiated and supervised the project. J.L. developed the model and performed simulations. All authors analyzed the data and wrote the manuscript.

*Address correspondence to: Hongyuan Jiang (jianghy@ustc.edu.cn).

Abbreviations used: 2D, two dimensional; 3D, three dimensional; TCJ, tricellular junction.

© 2019 Li *et al.* This article is distributed by The American Society for Cell Biology under license from the author(s). Two months after publication it is available to the public under an Attribution–Noncommercial–Share Alike 3.0 Unported Creative Commons License (<http://creativecommons.org/licenses/by-nc-sa/3.0>).

"ASCB®," "The American Society for Cell Biology®," and "Molecular Biology of the Cell®" are registered trademarks of The American Society for Cell Biology.

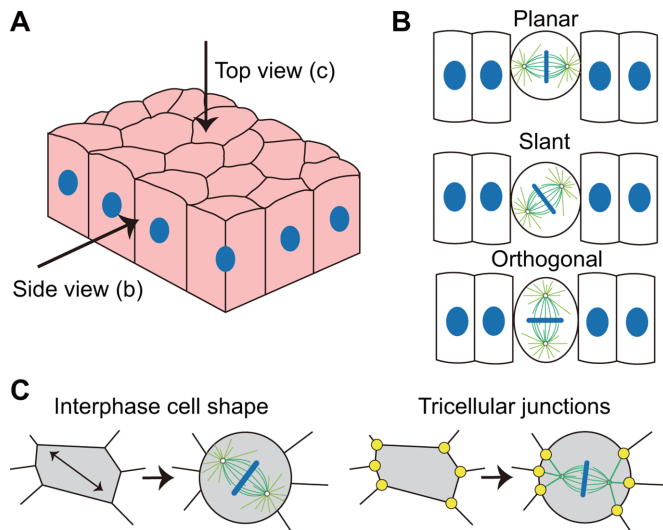


FIGURE 1: Schematics of the epithelial tissue and the mitotic spindle orientation. (A) Schematics of the epithelial tissue. (B) The spindle orientation is planar, slant, or orthogonal in the side view. (C) The spindle orientation within the tissue plane observed in the top view. It can be regulated by either the polygonal cell shape (Wyatt *et al.*, 2015) or the TCJs (Bosveld *et al.*, 2016).

(Figure 1, A and B). If the cell rounding is inhibited during the mitotic phase, the spindle could orient along the apico-basal axis due to the columnar shape of the epithelial cell (Chanet *et al.*, 2017). Furthermore, when one cell spreads on the two-dimensional substrate, the spindle orientation is usually parallel to the substrate due to the pulling of retraction fibers. When the cell is covered by another adhesive surface-coated fibronectin, the spindle orientation tends to be perpendicular to the substrate due to the symmetric distribution of traction fibers on both adhesive surfaces (Petridou and Skourides, 2014). Interestingly, if the cell is spreading on the substrate coated with E-cadherin as an artificial intercellular adhesion, the spindle orientation also becomes perpendicular to the substrate (Gloerich *et al.*, 2017). This might be induced by coupling the spindle orientation with the intercellular adhesion through E-cadherin, which can recruit the LGN/NuMA complex and apply pulling forces on microtubules through associated dyneins (Peyre *et al.*, 2011; Gloerich *et al.*, 2017; Wang *et al.*, 2018).

In addition to the competition between the planar and orthogonal directions (Figure 1B), the mitotic spindle of epithelial cells also need to select its horizontal orientation in the top view when the spindle is parallel to the tissue plane (Figure 1C). The spindles of epithelial cells, which usually have the polygonal shapes in the top view during the interphase, could orient either along their long axes (Wyatt *et al.*, 2015) or along the tricellular junction (TCJ) polarity (Bosveld *et al.*, 2016). The TCJs can act as force generators pulling astral microtubules and orienting cell division via the dynein-associated protein Mud (*Drosophila* homologue of NuMA) (Bosveld *et al.*, 2016). If the anisotropy of interphase cell shape is large, the spindle can orient along the long axis of the cell. In contrast, the spindle orientation could be predicted by the TCJ polarity more successfully when the anisotropy of interphase cell shape is small (Bosveld *et al.*, 2016). Moreover, when the cell monolayer is stretched, the spindle tends to orient along the long axis of the interphase cell shape (Hart *et al.*, 2017; Wyatt *et al.*, 2015). However, if the epithelial cell monolayer sustains a lower, more physiologically relevant uniaxial stretch (~12% strain), a part of spindles could align with the stretch axis

regardless of the long axis of the interphase cell shape (Hart *et al.*, 2017).

These experiments suggest that the intercellular adhesion and cell shape can both regulate the spindle orientation in epithelial cells. If their polarities are different, the two mechanisms may compete with each other. It has been shown that both the intercellular adhesion (Peyre *et al.*, 2011; Bosveld *et al.*, 2016; Chanet *et al.*, 2017; Gloerich *et al.*, 2017) and the cell shape (Théry and Bornens, 2006; Minc *et al.*, 2011; Pierre *et al.*, 2016; Li and Jiang, 2018) could orient the spindle by exerting forces on astral microtubules. Therefore, their cooperation or competition should be actually implemented by their resultant forces on the mitotic spindle. However, how these coupling mechanisms regulate the spindle orientation is still elusive.

In this paper, we use a general computational model to investigate how the spindle orientation is determined by the competition between the intercellular adhesion and cell shape in the top view and side view of the epithelial tissue (Figure 1). Our results not only quantitatively explain many existing experiment phenomena but also provide many interesting predictions that can be verified in future experiments.

RESULTS

The model reproduces the positioning and orientation of mitotic spindles in different cell shapes and adhesion geometries

The mitotic spindle is a bipolar structure consisting of large numbers of microtubules and various molecular motors (McIntosh *et al.*, 2012). We have developed a general model for mitotic spindles to study how cell size and cell shape regulate the positioning, orientation, and size regulation of mitotic spindles in our recent studies (Jiang, 2015; Li and Jiang, 2017, 2018). In this work, the original model is further improved (Figure 2, A and B), and we use two-dimensional (2D) simulations to investigate the orientation of mitotic spindles in different cell shapes and adhesion geometries. In brief, the model considers that microtubules are mainly nucleated from centrosomes and display dynamics, and the bipolar spindle structure can be kept stable through interactions among antiparallel microtubules and interactions between microtubules and chromosomes. Astral microtubules can interact with the cortex and generate pushing force by polymerization or pulling force by cortical dynein, so that the spindle can be positioned and oriented. Through dynamic simulation, we can reproduce the positioning and orientation of spindles (more details are provided in *Materials and Methods* and Supplemental Figures S1–S3 in the Supplemental Materials).

First, the cell is regarded as a sphere with the diameter of 20 μm during the mitotic phase in the model. The spindles in the simulation can always be positioned to the cell center from random initial conditions, but the spindle orientation is randomly distributed since the cell shape and the cortical parameters are isotropic (Supplemental Figure S4 and Supplemental Movie S1). To define a specific orientation, we elongate the cell to a stadium shape (Figure 2C and Supplemental Figure S5) or an elliptical shape (Supplemental Figure S6), corresponding to the compression of the round cell (Fischer-Friedrich *et al.*, 2014; Guild *et al.*, 2017) or the stretching of the tissue (Gibson *et al.*, 2011; Wyatt *et al.*, 2015), respectively. The cell aspect ratio λ , that is, the ratio of the long axis to the short axis, is 1.5, and the cell volume (actually the area in the 2D simulation) is same as the round cell. In these cases, the spindle can also be positioned successfully, but always oriented along the long axis of the cell independently of the initial conditions (Supplemental Figures S5 and S6; Supplemental Movie S2). Therefore, astral microtubules can

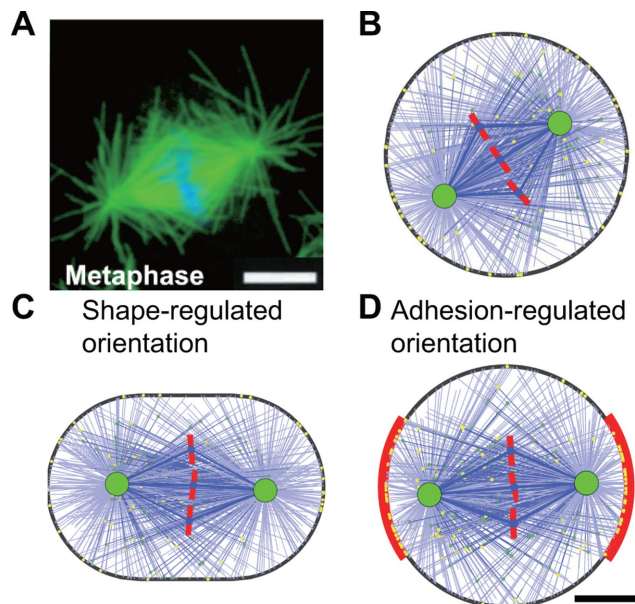


FIGURE 2: (A) A typical metaphase mitotic spindle observed in the experiment (Rogers *et al.*, 2002). Microtubules are labeled in green, and chromosomes are labeled in blue. (B) The simulated spindle in a round cell with the diameter of 20 μm (see also Supplemental Figure S4 and Supplemental Movie S1). (C) The simulated spindle in a stadium-shaped cell with the aspect ratio of 1.5 (see also Supplemental Figure S5 and Supplemental Movie S2). (D) The simulated spindle in a round cell with symmetric intercellular adhesion on the two sides (red region). The adhesive length $L = 12 \mu\text{m}$. The lateral adhesive region has a higher binding rate of cortical dynein than the other regions, and the ratio is $k = 11$ (see also Supplemental Figure S7). Scale bar: 5 μm .

effectively sense cell shape and control the spindle orientation along the long axis.

Then, we define two symmetric parts of the cortex as the intercellular adhesive regions on the mitotic rounding epithelial cell (Figure 2D). The E-cadherin on the lateral adhesion can recruit the LGN/NuMA complex (Peyre *et al.*, 2011; Gloerich *et al.*, 2017). The Par3/Par6/aPKC complex can exclude LGN from the apical cortex to the lateral cortex, which leads to apico-basal polarity (Hao *et al.*, 2010; Zheng *et al.*, 2010). Both mechanisms can result in the consequence that the lateral cortex has a higher level of LGN/NuMA than the apical cortex, and thereby the lateral pulling force is larger due to more associated dyneins (Seldin *et al.*, 2016). Therefore, we assume the lateral region has a much higher binding rate of cortical dynein than other regions (see *Materials and Methods*). It should also be noted that the distribution of LGN/NuMA complex can be changed by the cortical release and microtubule transport, but maintained by chromosome- and spindle-pole-derived signals after the spindle self-assembly (Kiyomitsu and Cheeseman, 2012; Zheng *et al.*, 2013). For simplicity, we assume the parameters of the lateral region are unchanged over time. The binding rate of cortical dynein at the lateral adhesive region is assumed $k = 11$ times larger than at the other regions, and the size of the lateral adhesion region is assumed as $L = 12 \mu\text{m}$. More values of these two parameters and their influences will be discussed in the later sections. In this case, the spindle can also be positioned successfully, and the spindle orientation is perpendicular to the lateral adhesive region, that is, along the adhesion polarity (Figure 2D and Supplemental Figure S7). Owing to the increase of binding rate of dyneins at the adhesion region, binding microtubules will assemble there so that the pulling force

generated at the adhesion region is larger than the other regions, and thus the spindle is pulled to orient along the adhesion direction. Therefore, either the cell shape or the intercellular adhesion geometry can regulate the spindle orientation in the simulation.

The competition between cell shape and bilateral intercellular adhesion determines spindle orientation in the side view of the epithelial tissue

Next, we consider the cell shape and the intercellular adhesion simultaneously to investigate the spindle orientation in the side view of Figure 1. The long axis of the columnar-shaped epithelial cell is usually along the apico-basal axis during the interphase, while the intercellular adhesion polarity is parallel to the tissue plane. If the cell rounding during the mitotic phase is inhibited, the cell shape remains elongated along the apico-basal axis, that is, perpendicular to the adhesion polarity (Chanet *et al.*, 2017). We consider such a case in the simulation to figure out whether the spindle orientation aligns with the apico-basal cell shape or the planar adhesion polarity. Experiments showed that the cell shapes in the side view are complex, but share a common feature that the long axis is along the apico-basal axis (Chanet *et al.*, 2017). Therefore, the cell shape is simplified as the stadium shape with a single long axis (Figure 3A).

It should be noted that the adhesive region actually covers the lateral cylindrical surface of the cell, but the adhesive region becomes the bilaterally symmetric segments of the cortex in the 2D simulations (Figure 3A). We show that the spindle orientation transits from the horizontal to the orthogonal direction with the increase of the cell aspect ratio as the cell area is constant (Figure 3B and Supplemental Movie S3). Specifically, when the aspect ratio is small, the intercellular adhesion dominates, and the spindle orientation is horizontal ($\lambda = 1.2$ in Figure 3B). When the aspect ratio is large, the cell shape dominates, and the spindle orientation is orthogonal, that is, along the apico-basal axis ($\lambda = 1.8$ in Figure 3B). When the aspect ratio is medium, the spindle orientation is controlled by both the intercellular adhesion and the cell shape, and thereby it is slanted ($\lambda = 1.4$ in Figure 3B). When the adhesion parameters are chosen as $k = 11$ and $L = 12 \mu\text{m}$, the results are in agreement with the experimental data from Chanet *et al.* (2017), where the cell rounding was inhibited to various degrees to control the cell aspect ratio (Figure 3C). The curve can be fitted by a sigmoidal function:

$$\alpha = \frac{\alpha^- - \alpha^+}{1 + e^{(\lambda - \lambda_T)/w_T}} + \alpha^+ \quad (1)$$

where α is the spindle orientation, that is, the angle between the spindle axis and the horizontal direction (Figure 3B); λ is the aspect ratio of cell shape; α^\pm are the limit values of the spindle orientation ($\alpha^- = 0$ and $\alpha^+ = \pi/2$); λ_T is the critical aspect ratio of cell shape, that is, the aspect ratio when $\alpha = (\alpha^- + \alpha^+)/2$; and w_T is a constant that reflects the width of the rising segment of the curve. Through fitting the experimental data (Chanet *et al.*, 2017) with the numerical simulation (Figure 3C), we obtain the critical aspect ratio $\lambda_T = 1.36$.

If the level of related proteins, such as E-cadherin or LGN/NuMA, is changed through the regulation of gene expression or corresponding chemical inhibitors (Peyre *et al.*, 2011; Gloerich *et al.*, 2017), the number of associated dyneins could be changed accordingly. To simulate this case, we can change the binding rate of cortical dyneins in the adhesive region. When the binding rate in the adhesive region is the same as the other region, that is, $k = 1$, the spindle orientation is completely decided by the cell shape ($\lambda_T \sim 1$). That is, as long as the aspect ratio λ is larger than 1, the spindle tends to orient along the orthogonal direction, that is, the long axis of the cell (black line in Figure 3D). With the increase of the binding

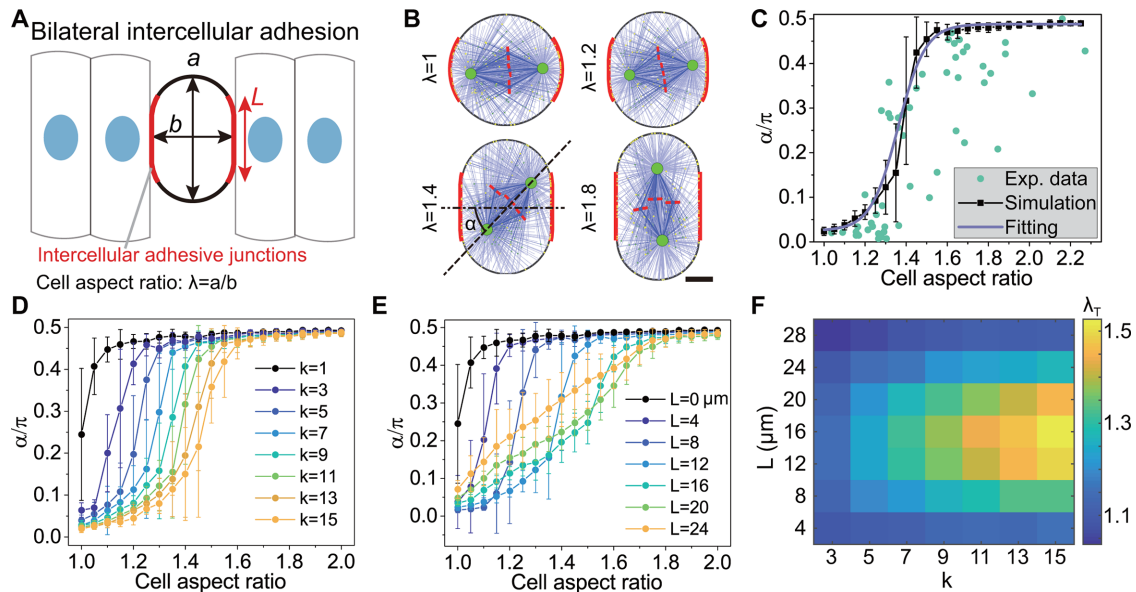


FIGURE 3: Regulating the spindle orientation via the cell shape and the bilateral intercellular adhesion in the side view. (A) The schematic shows the cell shape and intercellular adhesion of a dividing epithelial cell in the 2D simulation. The cell is stadium-shaped, where the red segments represent the intercellular adhesion region. (B) The snapshots of simulated spindles in the cells with different aspect ratios, but the same adhesive length and adhesive strength ($L = 12 \mu\text{m}$, $k = 11$) (see also Supplemental Movie S3). Scale bar: $5 \mu\text{m}$. (C) The spindle orientation quantified by the angle between the spindle axis and the adhesion polarity from (B) is plotted against the aspect ratio of the cell shape (mean \pm SE, 50 simulations for each case, the same below). The green dots are the experimental data from Chanet et al. (2017). The solid line is the fitting of the simulation results by using Eq. 1. (D) The role of the adhesive strength in governing the spindle orientation. (E) The role of the adhesive length in governing the spindle orientation. The curves in D and E can also be fitted by Eq. 1 (not shown). (F) Through fitting, the critical aspect ratio λ_T can be obtained, and it is the function of the adhesive strength k and adhesive length L .

rate k in the adhesive region, the critical aspect ratio λ_T increases (Figure 3D), which indicates that a stronger intercellular adhesion can ensure more planar division in the epithelial tissue.

Moreover, we also change the adhesive length in the simulation to investigate the influence of the size of the adhesion area on the spindle orientation. We find that the critical aspect ratio increases with the adhesive length only when $L \leq 12 \mu\text{m}$ (~20% of the cell perimeter; Figure 3E), but decreases if the adhesive length increases further (Figure 3E). This is because the polarity of the intercellular adhesion will be weakened when the adhesive length is too long and finally disappears when the whole cell is adhesive. Taken together, a strong adhesion and moderate adhesive length can generate a large critical aspect ratio λ_T , leading to more planar divisions in the epithelial tissue (Figure 3F).

Besides, we have investigated the role of other cortical parameters in the orientation process without adhesion in our recent work (Li and Jiang, 2018). To further investigate how the cortical parameters impact the spindle orientation when cell adhesion exists, we changed the unbinding rate of cortical dyneins as an example (Supplemental Figure S8). We find that the critical aspect ratio increases with the decrease of the unbinding rate. This is because the decrease of unbinding rate of dynein leads to the increase of the pulling–pushing ratio of cortical microtubules (Li and Jiang, 2018), and the adhesion polarity can have a stronger effect. Previously, we have also studied the spindle length regulation (Li and Jiang, 2017). Here we found that the critical aspect ratio increases with the spindle length through increasing the binding rate of cross-linking kinesins (Supplemental Figure S8). This indicates the adhesion polarity can have a stronger influence on the longer spindle.

It should be noted that the lateral adhesion region can be asymmetric due to the apico-basal cell polarity, that is, it is closer to the apical cortex during the interphase (Bergstrahl et al., 2013). During the mitotic phase, the asymmetry in the lateral adhesion region may remain the same if the cell rounding is inhibited. Therefore, we further assume the adhesive region is asymmetric with 75% of the adhesion region closer to the apical cortex (Supplemental Figure S9). We found the results are similar to the symmetric cases as expected.

The competition between unilateral cell adhesion on E-cadherin-coated substrate and compressed cell shape determines spindle orientation

Above, we have shown that the competition between the bilateral intercellular adhesion and the cell shape can determine the spindle orientation. We then wondered how the spindle orientation is determined if only one side of the cell adheres to others. Previous studies showed that when the cell adheres to the E-cadherin-coated wall as an artificial intercellular adhesion, the mitotic spindle orientation is perpendicular to the wall (Gloerich et al., 2017). To study this phenomenon, we assumed only the bottom of the cell is the adhesive region (Figure 4A). On the basis of the experimental observation (Gloerich et al., 2017), we assumed that the adhesive length of the round cell is $L = 7 \mu\text{m}$. Simulations show the spindle orientation can be perpendicular to the substrate, which is in good agreement with the experimental result (Gloerich et al., 2017) (the case $\lambda = 1$ in Figure 4B; Supplemental Movie S4). This result also confirms that the unilateral adhesion is enough to control the spindle orientation.

Then, we investigated the competition between the unilateral intercellular adhesion and cell shape. If we further use a nonadhesive surface, such as the cantilever beam of the atomic force

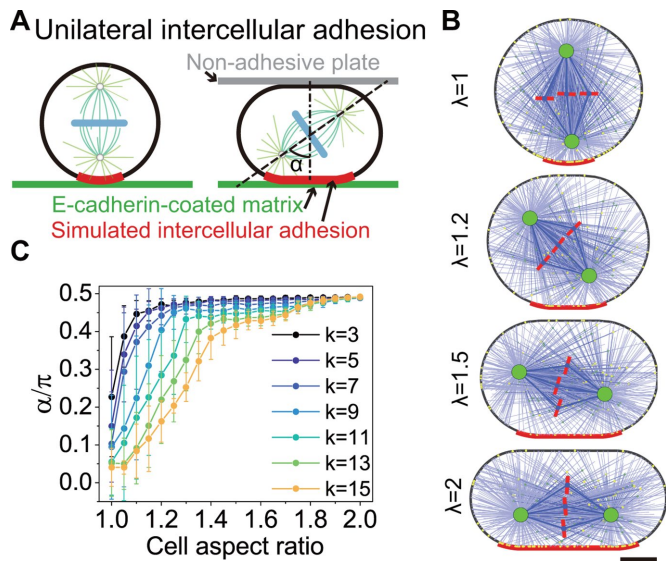


FIGURE 4: Regulating the spindle orientation via cell compression vs. unilateral intercellular adhesion in the side view. (A) The schematic shows the cell shape and the artificial intercellular adhesion on the E-cadherin-coated matrix in the 2D simulation. The compressing plate above is nonadhesive. The matrix below (green color) is E-cadherin-coated. The cell is stadium-shaped, where the adhesive length (red color) increases with the compression degree. (B) The snapshots of the simulated spindles in the cells with various aspect ratios but the same adhesion strength ($k = 11$) (see also Supplemental Movie S4). Scale bar: $5 \mu\text{m}$. (C) The spindle orientation is plotted against the aspect ratio of the cell with various adhesive strengths.

microscope or microplates, to compress the cell, the cell can elongate in the planar direction and the cell shape polarity could become perpendicular to the vertical adhesion polarity (Figure 4A). We assume that the adhesion area increases with the compression of the cell and further assume the adhesive region of the cell includes the cell surface whose distance to the substrate is less than $0.6 \mu\text{m}$ (Figure 4, A and B).

Similar to Figure 3, we also find the critical aspect ratio increases with the adhesive strength (Figure 4C). In other words, the stronger adhesion can orient more spindles perpendicular to the adhesion region. Unexpectedly, we find the spindle orientation angle α increases with the cell aspect ratio initially and then approaches two platforms one after the other (Figure 4C), especially for large k . After the first platform is reached, the cell shape dominates, with the result that the spindle tends to be parallel to the substrate. However, only one spindle pole is mainly pulled by the adhesive region due to the asymmetry of the adhesion, and thereby the spindle is slightly tilted ($\lambda = 1.5$ in Figure 4B). The first platform is slightly less than $\pi/2$. Until the adhesive length is longer than the spindle length, the two spindle poles are equally pulled by the adhesive region ($\lambda = 2$ in Figure 4B), and thus the spindle orientation can be parallel to the substrate completely and the second platform is reached. Compared with the bilateral adhesion (Figure 3), the spindle orientation with the unilateral adhesion is dominated by cell shape with a smaller aspect ratio, which indicates that the unilateral adhesion is relatively weaker to overcome the influence of cell shape than the bilateral adhesion.

As a comparison, we can also assume the adhesive length is independent of the cell shape (Figure 5). When the fixed adhesive length is small, the results are similar to Figure 4, that is, the spindle orientation can transit from vertical to parallel direction depending

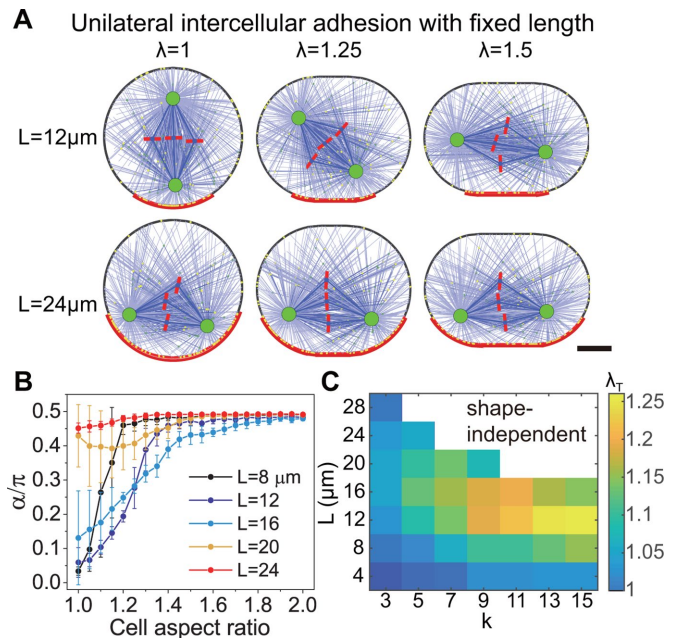


FIGURE 5: Regulating the spindle orientation via cell compression vs. unilateral intercellular adhesion with the fixed adhesive length. (A) Examples of the simulated spindles in the cells with short and long adhesive regions and various aspect ratios. The adhesive strength is $k = 11$. Scale bar: $5 \mu\text{m}$. (B) The spindle orientation is plotted against the aspect ratio of the cell with various adhesive lengths. (C) The curves of spindle orientation vs. cell aspect ratio can also be fitted by Eq. 1, and then the critical aspect ratios λ_T as the function of adhesive length and strength can be obtained. When the adhesive length is very large, the spindle orientation is always parallel to the substrate independently of the cell shape (white region).

on the degree of the compression of cell shape ($L = 12 \mu\text{m}$ in Figure 5A, $L \leq 16 \mu\text{m}$ in Figure 5B, and Supplemental Figure S11). We can also use Eq. 1 to fit the results to obtain the critical aspect ratio (Figure 5C) and then also find that a strong adhesion and moderate adhesive length can result in more adhesion-regulated spindle orientations, that is, perpendicular orientations. However, when the fixed adhesive length is large (up to one-half of cell perimeter), the spindle orientation will always be parallel to the substrate no matter what compression degree of the cell shape is ($L = 24 \mu\text{m}$ in Figure 5A, $L = 20$ and $24 \mu\text{m}$ in Figure 5B). This is because the adhesive length is always longer than the spindle length in this case, leading to equal pulling on both spindle poles by the unilateral adhesion (Figure 5A).

In addition, we also simulate the case of bilateral adhesion when the adhesive length increases with the cell elongation, and the results are qualitatively the same as the case of bilateral adhesion with the fixed length (Figure 3; Supplemental Figures S11 and S13). We also perform simulations in elliptical cells under the above conditions and find that the results are similar to the stadium-shaped cells (see the Supplemental Materials and Supplemental Figures S10–S13 for details).

The competition between the epithelial TCJs and cell shape determines the spindle orientation in the planar surface

Next, we consider the spindle orientation within the tissue plane (Figure 1C). During the interphase, epithelial cells usually have the polygonal shapes in the top view. In our recent work (Li and Jiang, 2018), we found that the final orientation of spindle is not necessarily

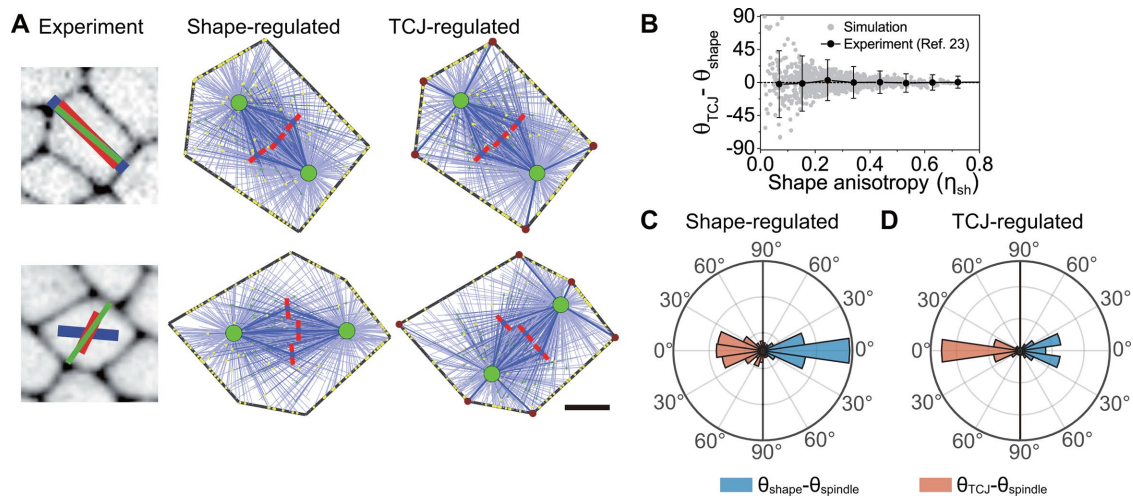


FIGURE 6: Modification of the model with the epithelial TCJs. (A) The comparison between experiments (Bosveld *et al.*, 2016) and simulations with and without the TCJ mechanism (also see Supplemental Movie S5). The blue, red, and green lines in the experimental images indicate the directions of the cell shape polarity, the TCJ polarity, and the actual spindle orientation, respectively. Scale bar: 5 μm . (B) We randomly generated 1000 polygonal cells and computed the directions of the cell shape polarity and the TCJ polarity. The distribution of the difference between the two directions ($\theta_{TCJ} - \theta_{shape}$) is in good agreement with the experimental data (Bosveld *et al.*, 2016). (C, D) The difference between the spindle orientation and the cell shape polarity (blue) or the TCJ polarity (red) obtained from the simulations with and without the TCJ mechanism.

along the longest axis in the polygonal cells, but is determined by the radial profile and the symmetry of the cell shape. This general rule can accurately predict the experimental results, in which the sea urchin embryos were forced into microchambers with various shapes (Minc *et al.*, 2011). However, since the epithelial cells in tissues become round during the mitotic phases, the cell shape would not be the main determinant of the spindle orientation. Bosveld *et al.* (2016) found that cells can memorize their interphase shapes by TCJs, which can also act as force generators pulling astral microtubules and orienting cell division via the dynein-associated protein Mud (*Drosophila* homologue of NuMA in mammals) (Bosveld *et al.*, 2016). Therefore, similar to the lateral adhesion, we assume the binding rate of dyneins at the TCJs is higher. Since the astral microtubules are distributed uniformly in the model, the number of microtubules that can reach TCJs are limited and less than the other cortical region. To ensure the sufficient influence of TCJs, we slightly increase the nucleation rate in the direction pointing to TCJs (see *Materials and Methods*). Since the cell completely adheres to surrounding cells from the top view, all the cell cortex except the TCJs are defined as the intercellular adhesion region ($k = 11$) as above.

To test the modified model, we select two typical cell shapes from the experiment (Bosveld *et al.*, 2016), in which the TCJ polarity and the cell shape polarity are consistent and inconsistent, respectively (Figure 6A). The definition of the TCJ polarity and the cell shape polarity is given in the Supplemental Materials (Bosveld *et al.*, 2016). Our simulations show that the spindle can orient along the cell shape polarity without the TCJ mechanism, but along the TCJ polarity with the TCJ mechanism (Figure 6A and Supplemental Movie S5). We further generate 1000 random polygons with the same area and compute the direction angles of the TCJ polarity θ_{TCJ} and the cell shape polarity θ_{shape} of these shapes. The variance of their difference $\theta_{TCJ} - \theta_{shape}$ decreases with the shape anisotropy, while the mean of $\theta_{TCJ} - \theta_{shape}$ keeps zero (Figure 6B). Through simulating the spindle orientation in these shapes, we find the TCJ polarity gives better predictions of the spindle orientation than the cell shape when the TCJ mechanism exists (Figure 6D), which is in

agreement with the experimental data (Bosveld *et al.*, 2016). Instead, if the TCJ mechanism is not considered, it is better to use the cell shape to predict the spindle orientation (Figure 6C).

We did not consider the cell rounding during the mitotic phase in the simulations above, because other detailed mechanism is needed to determine the junction positions after the cell rounding. Ideally, the cell shape polarity disappears after the cell rounding. However, in previous experiments, there exist some elliptical cells during the metaphase in the epithelial tissue (Nakajima *et al.*, 2013; Bosveld *et al.*, 2016; Wang *et al.*, 2017; Scarpa *et al.*, 2018) mainly due to the anisotropic distribution of mechanical stress on the mitotic cells (Gibson *et al.*, 2011; Wyatt *et al.*, 2015). For instance, in Figure 3C of Gibson *et al.* (2011), the spindle orientation is along the TCJ polarity, but perpendicular to the long axis of the elliptical cell. This showed that in this case, the TCJs dominate the spindle orientation when the cell shape polarity and the TCJ polarity are inconsistent. However, what if the cell shape anisotropy is larger?

To answer this question, we select a typical shape that the long axis of the ellipse is perpendicular to the TCJ polarity (Figure 7A). The anisotropy of TCJs can be changed by the distribution of the TCJs. As shown in Figure 7A, the TCJs are distributed symmetrically, the increase of the angle θ ($\theta \leq 30^\circ$) can result in the decrease of the TCJ anisotropy, and the anisotropy decreases to 0 when $\theta = 30^\circ$ (see the Supplemental Materials). We find that for the same TCJ anisotropy, if the anisotropy of the cell shape is small, the spindle orientation tends to be along the TCJ polarity; but if the anisotropy of the cell shape is large, the spindle orientation tends to be along the long axis of the cell (Figure 7A and Supplemental Movie S6). This indicates that the TCJs only dominate the spindle orientation for small anisotropy of the cell shape, which is similar to the circumstance of intercellular adhesion (Figure 3). In the experiments, for example, in Figure 3C of Gibson *et al.* (2011), the anisotropy of the cell shape is small ($\lambda \sim 1.25$), and thus the spindle orientation is along the TCJ polarity. As expected, when the TCJ anisotropy is decreased (i.e., θ is increased), or the pulling force generated at the TCJ is decreased, the critical aspect ratio of the cell decreases, that is, there

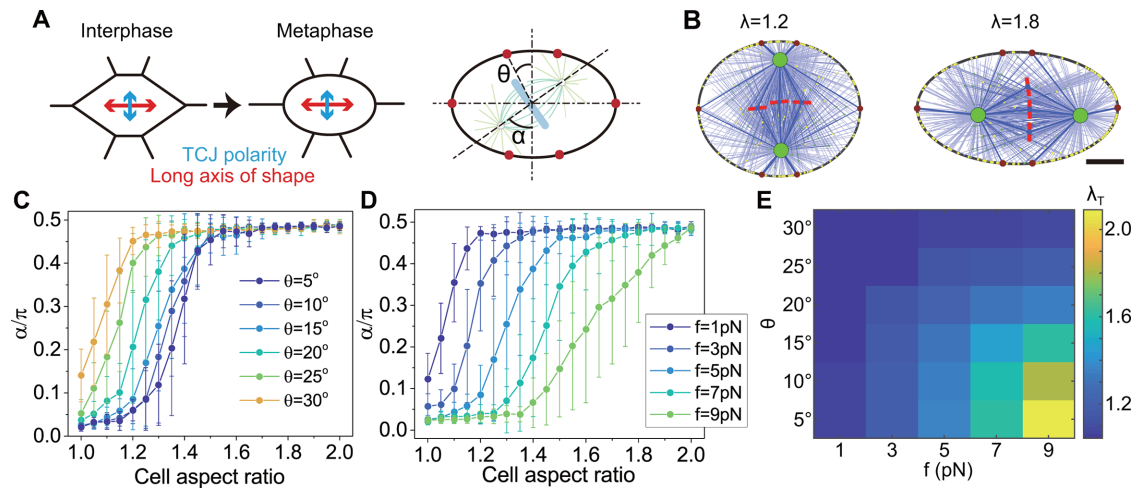


FIGURE 7: Regulating the spindle orientation via cell shape and TCJs in the top view. (A) When subjected to anisotropic stress, the rounding cell could exhibit an elliptical shape during the mitotic phase (Wyatt *et al.*, 2015), probably leading to the inconsistency of the TCJ polarity and the cell shape polarity. The schematic shows an example that the long axis of the elliptical cell is perpendicular to the TCJ polarity. (B) The snapshots of the simulated spindles in the cells with different aspect ratios but the same force and anisotropy of the TCJs ($f = 5 \text{ pN}$, $\theta = 15^\circ$). Scale bar: $5 \mu\text{m}$. (C) The spindle orientation is plotted against the aspect ratio of the cell shape with various anisotropy of the TCJs. (D) The spindle orientation is plotted against the aspect ratio of the cell shape with various forces generated at the TCJs. (E) The critical aspect ratio λ_T as the function of the anisotropy and the pulling force at the TCJs is obtained by using Eq. 1 to fit the curves in C and D and other cases.

are fewer spindles oriented along the TCJ polarity (Figure 7, C–E). The results of the stadium-shaped cells are also similar to the results of elliptical cells (Supplemental Figure S14).

DISCUSSION

In this work, we focused on the epithelial cell and considered both the cell shape and adhesion geometry to investigate the mitotic spindle orientation in the side view and top view of the epithelial tissue (Figure 1). The positioning and orientation of spindles are mainly driven by cortical forces on astral microtubules, including pushing force and pulling force. The combination of pushing force and pulling force can provide a more robust mechanism for positioning (Zhu *et al.*, 2010; Pavin *et al.*, 2012) and orientation (Li and Jiang, 2018). The cytoplasmic pulling by motors along microtubules can also drive the positioning and orientation, but this mechanism is only significant in very large cells during early embryonic development (Wühr *et al.*, 2010; Minc *et al.*, 2011; Li and Jiang, 2018). In normal body cells, the cytoplasmic pulling is negligible. With uniformly distributed astral microtubules, cortical forces on astral microtubules can generate a torque to rotate the spindle to the minimal torque orientation, that is, the long axis of the cell. The larger the cell shape anisotropy is, the stronger the torque becomes. In contrast, the cell adhesion, including the E-cadherin adhesion and TCJs, can induce preferential distribution of microtubules and generate a larger pulling force on microtubules in the adhesion region. The preferential pulling force can also generate torque to rotate the spindle to the direction of adhesion polarity. Shape-generated and adhesion-generated torques can be cooperative or competitive to control the spindle orientation. Therefore, we found that in epithelial cells, the intercellular adhesion dominates the spindle orientation for small anisotropy of the cell shape, but the cell shape dominates for large anisotropy of the cell shape (Figures 3 and 8A). When the cell adheres to the E-cadherin-coated wall as an artificial intercellular adhesion, the mitotic spindle orientation is perpendicular to the wall (Gloerich *et al.*, 2017) since the adhesion to the E-cadherin-coated surface leads to more pulling force pointing to the adhesion

region (Figure 8B). However, if a nonadhesive plate is used to compress the cell, the mitotic spindle may tilt or even become parallel to the surface due to the increase of anisotropy of the cell shape (Figures 4 and 8B). Therefore, the spindle orientation is determined by the competition between cell shape and the nonuniformly distributed force on the spindle induced by intercellular adhesion.

Compared to the E-cadherin-coated matrix (Gloerich *et al.*, 2017), cells that adhered to the FN-coated matrix (Petridou and Skourides, 2014) have different spindle orientations. In this case, the lateral retraction fibers can generate larger lateral pulling forces on astral microtubules after the cell rounding and thereby the spindle orientation parallels to the surface (Figure 8C). However, when the cell is covered by another FN-coated surface, the spindle orientation tends to be perpendicular to the substrate due to the symmetric distribution of traction fibers on the both adhesive surfaces (Petridou and Skourides, 2014). No matter whether the cells adhere to one or two parallel FN-coated surfaces, the spindle orientation can also be tuned by the cell shape if the cell shape is further changed by external forces (Figure 8C). Similarly, when cells adhere to various fibronectin micropatterns, although the cells still remain spherical after the mitotic cell rounding, the spindle orientation can be regulated effectively since the direction of the pulling force generated by the retraction fibers can be designed (Théry *et al.*, 2005).

Another way to induce the nonuniformly distributed astral microtubules and pulling forces is TCJs (Figures 7 and 8D), through which cells can memorize their interphase shapes via the dynein-associated protein Mud (Bosveld *et al.*, 2016). Finally, when the spindle is oriented by some polarized chemical signal (Siller and Doe, 2009; Williams and Fuchs, 2013), we speculate that the spindle orientation can also be changed if the cell is elongated perpendicular to the direction of polarization (Figure 8E). Therefore, the competition between cell shape and cell adhesion could exist under various mechanical microenvironments.

Our results are in agreement with some existing experiment observations (Bosveld *et al.*, 2016; Chanet *et al.*, 2017; Gloerich *et al.*, 2017). Moreover, we also provided more predictions that could be

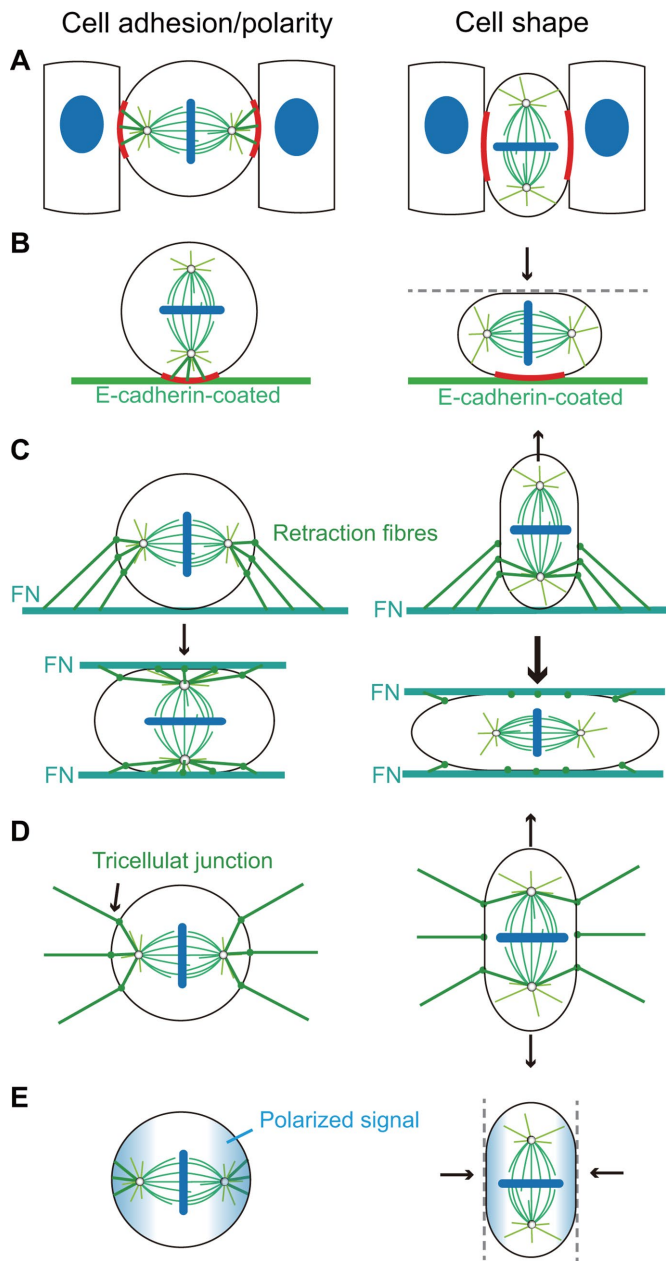


FIGURE 8: Mitotic spindle orientation is regulated by the competition between cell shape and cell adhesion geometry (or cell polarity) in various mechanical microenvironments, including (A) cells in the epithelium are adhered by surrounding cells; (B) cells are adhered on the E-cadherin-coated matrix; (C) cells are adhered on FN-coated matrix with retraction fibers; (D) cells are pulled by TCJs; (E) cells are polarized by chemical signals.

verified in future experiments. Among currently available experimental methods, the position and size of the adhesion can be controlled by microcontact printing (Théry *et al.*, 2005, 2007); the adhesive strength can be changed by inhibitors or regulation of gene expression; and the cell shape can be manipulated by microfabricated chambers (Minc *et al.*, 2011), atomic force microscope, or microplates (Petridou and Skourides, 2014). Therefore, based on the combination of these methods, our predictions can be further tested, and the competition between the cell shape and the adhesion geometry can be observed and investigated more directly and quantitatively.

The computational model used in this paper was developed based on our recent work (Jiang, 2015; Li and Jiang, 2017, 2018), and the new version is more general and robust after improvement. Most of the previous models for spindle orientation considered the spindle structure as a bipolar rigid body (Théry *et al.*, 2007; Gibson *et al.*, 2011; Minc *et al.*, 2011; Pierre *et al.*, 2016). In contrast to these phenomenological assumptions, we considered the formation of bipolar spindle structure and the capture and positioning of chromosomes based on the search-and-capture mechanism (Mogilner and Craig, 2010). Therefore, our model is more general. Although the formation of spindle structure is not necessary to the main conclusion of this paper, it is probably useful in future studies. For example, if the spindle size is changed by the pushing force generated by kinesin-5 or the pulling force on kinetochores, what is the influence on the spindle orientation? Besides, to improve computational efficiency, we used 2D simulations with minimal simplification from the 3D model. The competition we considered is between the planar and orthogonal orientation in Figure 3, or between the parallel direction and perpendicular direction to the substrate in Figures 4 and 5. Furthermore, the spindle orientation has already been confined to the tissue plane in Figures 6 and 7. Therefore, 2D simulation is enough for the problems we studied. We did not consider the deformation of microtubules explicitly and only recorded the state and force of microtubules as some previous models (Zhu *et al.*, 2010; Pavin *et al.*, 2012), which also largely increased the computational efficiency. Recent studies also found some new forces and structure in spindles, including the bridge, twist, and rotational forces (Kajtez *et al.*, 2016; Novak *et al.*, 2018; Tolíc *et al.*, 2019), which we did not consider in the current model. In the future, we can include them in our model by considering the deformation of the microtubules.

MATERIALS AND METHODS

We have developed a general computational model for mitotic spindles in our recent work (Li and Jiang, 2017, 2018). In the model, microtubules are mainly nucleated from two centrosomes and grow or shrink by the polymerization or depolymerization of their positive ends (Zhu *et al.*, 2010). Thus, they display the dynamic instability to search the kinetochores on the chromosomes (Mogilner and Craig, 2010). The polymerization of microtubules can generate pushing forces on the cortex or chromosome arms (Civelekoglu-Scholey *et al.*, 2006; Pavin *et al.*, 2012), and the depolymerization can generate pulling forces on the kinetochore (Civelekoglu-Scholey *et al.*, 2006; Banigan *et al.*, 2015). In the meantime, microtubules can be bound by cortical motors (Mogilner and Craig, 2010), chromokinesins (Campas and Sens, 2006), cytoplasmic motors (Wu'hr *et al.*, 2010), and sliding motors (Nédélec, 2002; Goshima *et al.*, 2005b; Channels *et al.*, 2008; Loughlin *et al.*, 2010), all of which can generate various forces on the microtubules (Supplemental Figure S1). Relying on these forces, the spindle can be self-assembled, positioned to the cell center, and oriented along the cell long axis (Li and Jiang, 2017, 2018). Here, we further improved the model to investigate the spindle orientation.

Nucleation and dynamic instability of microtubules

During the self-assembly of mitotic spindles, microtubules can be nucleated from the centrosome, or near the chromosomes (Karsenti and Nédélec, 2004), or from existing microtubules as branches in the spindle region (Petry *et al.*, 2013) (Inset 1 of Supplemental Figure S1). The microtubules nucleated near the chromosomes are converged to the spindle pole by minus end-directed motor proteins, dynein and Ncd (Goshima *et al.*, 2005a), and the branching

microtubules have the same polarity with their mother microtubules (Petry *et al.*, 2013). Therefore, all microtubules have interactions with the spindle poles. For simplicity, we assume all microtubules are nucleated from the centrosomes as we did before (Li and Jiang, 2017), and there is a higher nucleation rate in the direction from the centrosome to chromosomes. Specifically, in the 2D model, we first assume that each centrosome has a nucleation rate of k_0 and the nucleation direction is uniformly distributed. Therefore, the density of nucleation rate is $k_0/(2\pi)$. Second, we assume that the density of nucleation rate in the direction from the centrosome to chromosomes is higher as $k_n k_0/(2\pi)$, where k_n is a constant parameter and larger than 1 (Inset 1 of Supplemental Figure S1). This assumption is more reasonable than the original model in which we assumed the extra nucleation in a range of 60° (Li and Jiang, 2017). The positioning and orientation of spindles are regulated by astral microtubules, which are mainly generated by the nucleation rate of k_0 in the model, and the extra nucleation can ensure the bipolar spindle structure is stable.

Microtubules can randomly switch between slowly growing state and fast shrinking state, which is named the dynamic instability and crucial to searching the kinetochore (Mogilner and Craig, 2010). Here, we assume that the microtubules elongate at a speed of v_1 in the growing state and shorten at a speed of v_2 in the shrinking state. The rescue rate (from shrinking to growing) and catastrophe rate (from growing to shrinking) of microtubules are k_1 and k_2 , respectively. These four parameters determine the dynamics of microtubules and are considered as constants in the cytoplasm.

Microtubules interact with cortex

When a growing microtubule reaches the cortex, its polymerization is blocked, and a pushing force is generated on the cortex (Pavin *et al.*, 2012) (Inset 3 of Supplemental Figure S1). The pushing force equals the stall force of microtubules f_{stall} . Since the microtubules are very slender (length $\sim 10 \mu\text{m}$, diameter 25 nm), they can be buckled by the pushing force easily (Pavin *et al.*, 2012). If we neglect the lateral limitation, the critical force is given by the Euler buckling formula $f_c = \pi^2 \kappa / l^2$, where κ and l denote the bending rigidity and the length of the microtubule, respectively (Pavin *et al.*, 2012; Jiang, 2015; Li and Jiang, 2017). After buckling, the growth of the microtubule only brings a little increase of the pushing force, thus we assume the pushing force equals the critical buckling force when the microtubule is buckling (Jiang, 2015). Therefore, the pushing force induced by microtubule polymerization is given as

$$f^+ = \min(f_{\text{stall}}, \pi^2 \kappa / l^2) \quad (2)$$

When the microtubules are applied with a pushing force by the cortex, they have a higher catastrophe rate k_2^* (Howard, 2006; Kozlowski *et al.*, 2007).

Besides the pushing force, the cortex can also apply pulling force on microtubules generated by cortical dynein (Inset 3 of Supplemental Figure S1), and the pulling force is crucial to the positioning and orientation of mitotic spindles (Laan *et al.*, 2012; Bosveld *et al.*, 2016; Gloerich *et al.*, 2017). The cortical dynein can bind to microtubules touching the cortex at a rate of $k_{\bar{v}}$, which is usually thought to be proportional to the density of unbound motors. We assume the density of cortical dyneins is uniform, so that $k_{\bar{v}}$ is constant on the cortex. When the cortical microtubule is bound by cortical dynein, the dynein can walk to the minus-end direction of the microtubule driven by the energy of the hydrolysis of ATP and thus generate a pulling force on the microtubule. The force is velocity-dependent as (Jiang, 2015; Li and Jiang, 2017)

$$f^- = f_{\bar{v}} \left(1 - \frac{v^-}{v_{\bar{v}}}\right) \quad (3)$$

where $f_{\bar{v}}$ and $v_{\bar{v}}$ are the stall force and the unloaded velocity of dynein; v^- is the walking velocity of the motor. If we neglect the poleward flux of microtubules, the velocity here equals the velocity component of the centrosome in the microtubule direction. It should be noted that the velocity is positive when the microtubule is shortening, while it is negative when the microtubule is elongating.

The binding dynein can unbind from the microtubule at a rate of $k_{\bar{u}}$, which is load-dependent (Campas and Sens, 2006; Jiang, 2015; Li and Jiang, 2017), as

$$k_{\bar{u}} = k_{\bar{u}}^0 e^{f^- / f_{\bar{u}}} \quad (4)$$

where $f_{\bar{u}}$ is a characteristic force representing the sensitivity of the unbinding rate to the load, and $k_{\bar{u}}^0$ is the unloaded unbinding rate of dynein. After the unbinding of dynein, the microtubules are in the state of depolymerization (Laan *et al.*, 2012).

Force generated by cytoplasmic dyneins

Besides above-mentioned motors, some motors walk along the microtubules to carry cargoes in the cytoplasm (Inset 6 in Supplemental Figure S1). These motors mainly generate pulling forces and also play an important role in the positioning and orienting of mitotic spindles (Wühr *et al.*, 2010; Minc *et al.*, 2011; Li and Jiang, 2018). This cytoplasmic pulling force is thought as microtubule length-dependent because more motors can bind to a longer microtubule. It should be noted that the number of binding motors is large, but the velocity of one motor carrying a cargo and walking along the microtubule almost equals the unloaded velocity, which indicates the pulling force generated by a single motor is very small (Eq. 3). Therefore, we simply assume the pulling force induced by the cytoplasmic motors on a microtubule is

$$f_{\bar{d}} = \eta l \quad (5)$$

where η is the pulling force per unit microtubule length and l is the total length of the microtubule (Li and Jiang, 2017, 2018).

Force generated at the intercellular adhesion region

Experiment studies have found that the E-cadherin can recruit the LGN/NuMA complex (Gloerich *et al.*, 2017; Wang *et al.*, 2018). They can bind more astral microtubules and apply larger pulling forces through associated dyneins (Seldin *et al.*, 2016). Since we have assumed the binding rate of dyneins is proportional to the density of unbound motors, we can assume that the intercellular adhesion region has a higher binding rate of dyneins, which is k times higher than that on the other cortex region. The forces generated on microtubules and the other changes of microtubule state are the same as described above (Eqs. 2–4).

Force generated at TCJs

The TCJs can also act as force generators to pull astral microtubules and orient cell division via the dynein-associated protein Mud (Bosveld *et al.*, 2016). When microtubules arrive at the TCJ, defined as the region where the distance from the node is less than $0.25 \mu\text{m}$, they can bind to dyneins at the TCJs at a larger binding rate of $k_{b,a}$. However, microtubules are distributed uniformly, and microtubules that can reach the TCJs are limited and less than the other cortex region. Under such conditions, the influence of TCJs on the spindle is little. Therefore, we assume there is an extra nucleation rate $k_l k_0$

along the existing microtubules that have been bound to TCJs to increase the number of microtubules there. Since the extra nucleation rate is much smaller than k_0 , the total number of cortical microtubules is almost unchanged. The force generated by TCJs on microtubules is also similar to the cortical dynein, $f_a^- = f(1 - v^- / v_0^-)$. Here, f is the stall force generated by the motor at TCJs and will be regulated as a controlling parameter in the simulations. Besides, this binding can also unbind at a load-dependent rate as Eq. 4.

Bipolar spindle structure and other simulation details

Based on these mechanical interactions above, the spindle can be positioned and oriented by the cortical cues. Besides, through the interaction between antiparallel microtubules, and the interaction between microtubules and chromosomes based on the search-and-capture mechanism (Mogilner and Craig, 2010), the bipolar spindle structure can keep stable. More details of model and simulation methods can be seen in the Supplemental Materials.

Compared with the original model, the new version mainly has three improvements. First, in the original 2D model, chromosomes could hinder most of the microtubules from forming antiparallel structures. Therefore, we computed the chromosomes and antiparallel microtubules separately and then superposed them. However, in the 3D case, chromosomes have a finite thickness and thus can only hinder a fraction of microtubules. Thus, we can directly simulate the antiparallel microtubules. Considering the computational feasibility, we still use 2D simulation with a quasi-3D assumption that microtubules can bypass the chromosome. Therefore, they cannot only bind to chromosomes by chromokinesins or kinetochores but also bind to antiparallel microtubules by cross-linkers (Supplemental Figure S1). Second, microtubules can be nucleated from centrosomes, chromosomes (Karsenti and Nédélec, 2004), or existing microtubules as branches in the spindle region (Petry *et al.*, 2013). The latter two nucleation sites can induce more polar microtubules between the centrosome and chromosomes. For simplicity, we still assume all microtubules are nucleated from centrosomes (Li and Jiang, 2017, 2018), but the nucleation rate is given higher in the range where the microtubule can meet the chromosomes. In this way, the simulated spindle has a higher density of polar microtubules than that of astral microtubules (Supplemental Figure S2), which is more consistent with the real spindle. Third, we add the microtubule bundling mechanism that the minus-end-directed molecular motor kinesin-14 can cooperate with the plus-end tracker EB1 to guide the growing plus end along the existing microtubule (Molodtsov *et al.*, 2016) (Supplemental Figure S1). We assume the microtubule connected on the kinetochore can induce this bundling mechanism. After these improvements, we can perform the dynamic Monte Carlo simulation (Supplemental Figure S3). More details of the model, simulation methods, and parameters (Supplemental Table S1) are provided in the Supplemental Materials.

ACKNOWLEDGMENTS

This work was supported by the National Natural Science Foundation of China (Grants No. 11622222, 11872357, and 11472271), the Thousand Young Talents Program of China, Fundamental Research Funds for the Central Universities, and the Strategic Priority Research Program of the Chinese Academy of Sciences (Grant No. XDB22040403).

REFERENCES

Banigan EJ, Chiou KK, Ballister ER, Mayo AM, Lampson MA, Liu AJ (2015). Minimal model for collective kinetochore-microtubule dynamics. *Proc Natl Acad Sci USA* 112, 12699–12704.

Bergstrahl DT, Lovegrove HE, St Johnston D (2013). Discs large links spindle orientation to apical-basal polarity in drosophila epithelia. *Curr Biol* 23, 1707–1712.

Bosveld F, Markova O, Guirao B, Martin C, Wang Z, Pierre A, Balakireva M, Gague I, Ainslie A, Christophorou N, *et al.* (2016). Epithelial tricellular junctions act as interphase cell shape sensors to orient mitosis. *Nature* 530, 495–498.

Campas O, Sens P (2006). Chromosome oscillations in mitosis. *Phys Rev Lett* 97, 128102.

Caussinus E, Gonzalez C (2005). Induction of tumor growth by altered stem-cell asymmetric division in drosophila melanogaster. *Nat Genet* 37, 1125–1129.

Chanet S, Sharan R, Khan Z, Martin AC (2017). Myosin 2-induced mitotic rounding enables columnar epithelial cells to interpret cortical spindle positioning cues. *Curr Biol* 27, 3350–3358.

Channels WE, Nédélec FJ, Zheng Y, Iglesias PA (2008). Spatial regulation improves antiparallel microtubule overlap during mitotic spindle assembly. *Biophys J* 94, 2598–2609.

Civelekoglu-Scholey G, Sharp D, Mogilner A, Scholey J (2006). Model of chromosome motility in drosophila embryos: adaptation of a general mechanism for rapid mitosis. *Biophys J* 90, 3966–3982.

di Pietro F, Echard A, Morin X (2016). Regulation of mitotic spindle orientation: an integrated view. *EMBO Rep* 17, 1106–1130.

Finegan TM, Na D, Cammarota C, Skeeters AV, Na'dasi TJ, Dawney NS, Fletcher AG, Oakes PW, Bergstrahl DT (2019). Tissue tension and not interphase cell shape determines cell division orientation in the drosophila follicular epithelium. *EMBO J* 38, e100072.

Fink J, Carpi N, Betz T, B'etard A, Chebah M, Azioune A, Bornens M, Sykes C, Fetler L, Cuvelier D, *et al.* (2011). External forces control mitotic spindle positioning. *Nat Cell Biol* 13, 771–778.

Fischer-Friedrich E, Hyman AA, Jülicher F, Müller DJ, Helenius J (2014). Quantification of surface tension and internal pressure generated by single mitotic cells. *Sci Rep* 4, 6213.

Gibson WT, Veldhuis JH, Rubinstein B, Cartwright HN, Perrimon N, Brodland GW, Nagpal R, Gibson MC (2011). Control of the mitotic cleavage plane by local epithelial topology. *Cell* 144, 427–438.

Gillies TE, Cabernard C (2011). Cell division orientation in animals. *Curr Biol* 21, R599–R609.

Gloerich M, Bianchini JM, Siemers KA, Cohen DJ, Nelson WJ (2017). Cell division orientation is coupled to cell-cell adhesion by the e-cadherin/Ign complex. *Nat Commun* 8, 13996.

Goshima G, Nédélec F, Vale RD (2005a). Mechanisms for focusing mitotic spindle poles by minus end-directed motor proteins. *J Cell Biol* 171, 229–240.

Goshima G, Wollman R, Stuurman N, Scholey JM, Vale RD (2005b). Length control of the metaphase spindle. *Curr Biol* 15, 1979–1988.

Guild J, Ginzberg MB, Hueschen CL, Mitchison TJ, Dumont S (2017). Increased lateral microtubule contact at the cell cortex is sufficient to drive mammalian spindle elongation. *Mol Biol Cell* 28, 1975–1983.

Hao Y, Du Q, Chen X, Zheng Z, Balsbaugh JL, Maitra S, Shabanowitz J, Hunt DF, Macara IG (2010). Par3 controls epithelial spindle orientation by apkc-mediated phosphorylation of apical pins. *Curr Biol* 20, 1809–1818.

Hart KC, Tan J, Siemers KA, Sim JY, Pruitt BL, Nelson WJ, Gloerich M (2017). E-cadherin and Ign align epithelial cell divisions with tissue tension independently of cell shape. *Proc Natl Acad Sci USA* 114, E5845–E5853.

Hertwig O (1884). Das problem der befruchtung und der isotropie des eies. eine theorie der vererbung. *Jenaische Zeitschrift für Naturwissenschaft* 18, 276–318.

Howard J (2006). Elastic and damping forces generated by confined arrays of dynamic microtubules. *Phys Biol* 3, 54.

Jiang H (2015). Cell size modulates oscillation, positioning and length of mitotic spindles. *Sci Rep* 5, 10504.

Kajtez J, Solomatina A, Novak M, Polak B, Vukušić K, Rüdiger J, Cojoc G, Milas A, Šestak IŠ, Risteski P, *et al.* (2016). Overlap microtubules link sister k-fibres and balance the forces on bi-oriented kinetochores. *Nat Commun* 7, 10298.

Karsenti E, Nédélec F (2004). The mitotic spindle and actin tails. *Biol Cell* 96, 237–240.

Kiyomitsu T, Cheeseman IM (2012). Chromosome- and spindle-pole-derived signals generate an intrinsic code for spindle position and orientation. *Nat Cell Biol* 14, 311.

Kozłowski C, Srayko M, Nedelec F (2007). Cortical microtubule contacts position the spindle in *C. elegans* embryos. *Cell* 129, 499–510.

Laan L, Pavin N, Husson J, Romet-Lemonne G, Van Duijn M, López MP, Vale RD, Jülicher F, Reck-Peterson SL, Dogterom M (2012). Cortical dynein

- controls microtubule dynamics to generate pulling forces that position microtubule asters. *Cell* 148, 502–514.
- Lancaster MA, Knoblich JA (2012). Spindle orientation in mammalian cerebral cortical development. *Curr Opin Neurobiol* 22, 737–746.
- Li J, Jiang H (2017). Geometric asymmetry induces upper limit of mitotic spindle size. *Biophys J* 112, 1503–1516.
- Li J, Jiang H (2018). Regulating positioning and orientation of mitotic spindles via cell size and shape. *Phys Rev E* 97, 012407.
- Loughlin R, Heald R, Nédélec F (2010). A computational model predicts *Xenopus* meiotic spindle organization. *J Cell Biol* 191, 1239–1249.
- Matsumura S, Kojidani T, Kamioka Y, Uchida S, Haraguchi T, Kimura A, Toyoshima F (2016). Interphase adhesion geometry is transmitted to an internal regulator for spindle orientation via caveolin-1. *Nat Commun* 7, ncomms11858.
- McIntosh JR, Molodtsov MI, Ataullakhanov FI (2012). Biophysics of mitosis. *Q Rev Biophys* 45, 147–207.
- Minc N, Burgess D, Chang F (2011). Influence of cell geometry on division-plane positioning. *Cell* 144, 414–426.
- Mogilner A, Craig E (2010). Towards a quantitative understanding of mitotic spindle assembly and mechanics. *J Cell Sci* 123, 3435–3445.
- Molodtsov MI, Mieck C, Dobbelaere J, Dammermann A, Westermann S, Vaziri A (2016). A force-induced directional switch of a molecular motor enables parallel microtubule bundle formation. *Cell* 167, 539–552.
- Nédélec F (2002). Computer simulations reveal motor properties generating stable antiparallel microtubule interactions. *J Cell Biol* 158, 1005–1015.
- Nakajima YI, Meyer EJ, Kroesen A, McKinney SA, Gibson MC (2013). Epithelial junctions maintain tissue architecture by directing planar spindle orientation. *Nature* 500, 359–362.
- Novak M, Polak B, Simunić J, Boban Z, Kuzmić B, Thomae AW, Tolić IM, Pavin N (2018). The mitotic spindle is chiral due to torques within microtubule bundles. *Nat Commun* 9, 3571.
- O’Connell CB, Wang YL (2000). Mammalian spindle orientation and position respond to changes in cell shape in a dynein-dependent fashion. *Mol Biol Cell* 11, 1765–1774.
- Pavin N, Laan L, Ma R, Dogterom M, Jülicher F (2012). Positioning of microtubule organizing centers by cortical pushing and pulling forces. *New J Phys* 14, 105025.
- Pease JC, Tirnauer JS (2011). Mitotic spindle misorientation in cancer-out of alignment and into the fire. *J Cell Sci* 124, 1007–1016.
- Petridou NI, Skourides PA (2014). Fak transduces extracellular forces that orient the mitotic spindle and control tissue morphogenesis. *Nat Commun* 5, 5240.
- Petry S, Groen AC, Ishihara K, Mitchison TJ, Vale RD (2013). Branching microtubule nucleation in *xenopus* egg extracts mediated by augmin and tpx2. *Cell* 152, 768–777.
- Peyre E, Jaouen F, Saadaoui M, Haren L, Merdes A, Durbec P, Morin X (2011). A lateral belt of cortical lgn and numa guides mitotic spindle movements and planar division in neuroepithelial cells. *J Cell Biol* 193, 141–154.
- Pierre A, Sallé J, Wühr M, Minc N (2016). Generic theoretical models to predict division patterns of cleaving embryos. *Dev Cell* 39, 667–682.
- Ragkousi K, Gibson MC (2014). Cell division and the maintenance of epithelial order. *J Cell Biol* 207, 181–188.
- Rogers SL, Rogers GC, Sharp DJ, Vale RD (2002). *Drosophila* eb1 is important for proper assembly, dynamics, and positioning of the mitotic spindle. *J Cell Biol* 158, 873–884.
- Scarpa E, Finet C, Blanchard GB, Sanson B (2018). Actomyosin-driven tension at compartmental boundaries orients cell division independently of cell geometry in vivo. *Dev Cell* 47, 727–740.
- Seldin L, Muroyama A, Lechler T (2016). Numa-microtubule interactions are critical for spindle orientation and the morphogenesis of diverse epidermal structures. *Elife* 5, e12504.
- Siller KH, Doe CQ (2009). Spindle orientation during asymmetric cell division. *Nat Cell Biol* 11, 365–374.
- Strauss B, Adams RJ, Papalopulu N (2006). A default mechanism of spindle orientation based on cell shape is sufficient to generate cell fate diversity in polarised *xenopus* blastomeres. *Development* 133, 3883–3893.
- Théry M, Jiménez-Dalmaroni A, Racine V, Bornens M, Jülicher F (2007). Experimental and theoretical study of mitotic spindle orientation. *Nature* 447, 493–496.
- Théry M, Racine V, Pépin A, Piel M, Chen Y, Sibarita JB, Bornens M (2005). The extracellular matrix guides the orientation of the cell division axis. *Nat Cell Biol* 7, 947–953.
- Théry M, Bornens M (2006). Cell shape and cell division. *Curr Opin Cell Biol* 18, 648–657.
- Tolić IM, Novak M, Pavin N (2019). Helical twist and rotational forces in the mitotic spindle. *Biomolecules* 9, 132.
- Wang X, Dong B, Zhang K, Ji Z, Cheng C, Zhao H, Sheng Y, Li X, Fan L, Xue W, et al. (2018). E-cadherin bridges cell polarity and spindle orientation to ensure prostate epithelial integrity and prevent carcinogenesis in vivo. *PLoS Genet* 14, e1007609.
- Wang MF, Hunter MV, Wang G, McFaul C, Yip CM, Fernandez-Gonzalez R (2017). Automated cell tracking identifies mechanically oriented cell divisions during *drosophila* axis elongation. *Development* 144, 1350–1361.
- Williams SE, Beronja S, Pasolli HA, Fuchs E (2011). Asymmetric cell divisions promote notch-dependent epidermal differentiation. *Nature* 470, 353–358.
- Williams SE, Fuchs E (2013). Oriented divisions, fate decisions. *Curr Opin Cell Biol* 25, 749–758.
- Wühr M, Tan ES, Parker SK, Detrich HW, Mitchison TJ (2010). A model for cleavage plane determination in early amphibian and fish embryos. *Curr Biol* 20, 2040–2045.
- Wyatt TP, Harris AR, Lam M, Cheng Q, Bellis J, Dimitracopoulos A, Kabla AJ, Charras GT, Baum B (2015). Emergence of homeostatic epithelial packing and stress dissipation through divisions oriented along the long cell axis. *Proc Natl Acad Sci USA* 112, 5726–5731.
- Xiong F, Ma W, Hiscock TW, Mosaliganti KR, Tentner AR, Brakke KA, Rannou N, Gelas A, Souhait L, Swinburne IA, et al. (2014). Interplay of cell shape and division orientation promotes robust morphogenesis of developing epithelia. *Cell* 159, 415–427.
- Zheng Z, Wan Q, Liu J, Zhu H, Chu X, Du Q (2013). Evidence for dynein and astral microtubule-mediated cortical release and transport of α i/lgn/numa complex in mitotic cells. *Mol Biol Cell* 24, 901–913.
- Zheng Z, Zhu H, Wan Q, Liu J, Xiao Z, Siderovski DP, Du Q (2010). Lgn regulates mitotic spindle orientation during epithelial morphogenesis. *J Cell Biol* 189, 275–288.
- Zhu J, Burakov A, Rodionov V, Mogilner A (2010). Finding the cell center by a balance of dynein and myosin pulling and microtubule pushing: a computational study. *Mol Biol Cell* 21, 4418–4427.